

## LYMPHOID NEOPLASIA

# CCND2 and CCND3 hijack immunoglobulin light-chain enhancers in cyclin D1<sup>-</sup> mantle cell lymphoma

David Martín-García,<sup>1,2,\*</sup> Alba Navarro,<sup>1,2,\*</sup> Rafael Valdés-Mas,<sup>3</sup> Guillem Clot,<sup>1,2</sup> Jesús Gutiérrez-Abril,<sup>3</sup> Miriam Prieto,<sup>1,2</sup> Inmaculada Ribera-Cortada,<sup>4</sup> Renata Woroniecka,<sup>5</sup> Grzegorz Rymkiewicz,<sup>6</sup> Susanne Bens,<sup>7,8</sup> Laurence de Leval,<sup>9</sup> Andreas Rosenwald,<sup>10,11</sup> Judith A. Ferry,<sup>12</sup> Eric D. Hsi,<sup>13</sup> Kai Fu,<sup>14,15</sup> Jan Delabie,<sup>16,17</sup> Dennis Weisenburger,<sup>18</sup> Daphne de Jong,<sup>19</sup> Fina Climent,<sup>20</sup> Sheila J. O'Connor,<sup>21</sup> Steven H. Swerdlow,<sup>22</sup> David Torrents,<sup>23,24</sup> Sergi Beltran,<sup>25</sup> Blanca Espinet,<sup>26,27</sup> Blanca González-Farré,<sup>2,28</sup> Luis Veloza,<sup>28</sup> Dolors Costa,<sup>2,28</sup> Estella Matutes,<sup>28</sup> Reiner Siebert,<sup>7,8</sup> German Ott,<sup>29,30</sup> Leticia Quintanilla-Martinez,<sup>31</sup> Elaine S. Jaffe,<sup>32</sup> Carlos López-Otín,<sup>2,3</sup> Itziar Salaverria,<sup>1,2</sup> Xose S. Puente,<sup>2,3,†</sup> Elias Campo,<sup>1,2,28,33,†</sup> and Sílvia Bea<sup>1,2,†</sup>

<sup>1</sup>Institut d'Investigacions Biomèdiques August Pi i Sunyer (IDIBAPS), Barcelona, Spain; <sup>2</sup>Centro de Investigación Biomédica en Red de Cáncer (CIBERONC), Madrid, Spain; <sup>3</sup>Departamento de Bioquímica y Biología Molecular, Instituto Universitario de Oncología, Universidad de Oviedo, Oviedo, Spain; <sup>4</sup>Hospital Nostra Senyora de Meritxell, Escaldes-Engordany, Andorra; <sup>5</sup>Cytogenetic Laboratory and <sup>6</sup>Department of Pathology and Laboratory Diagnostics, Maria Skłodowska-Curie Institute–Oncology Center, Warsaw, Poland; <sup>7</sup>Institute of Human Genetics, Ulm University Medical Center, Ulm University, Ulm, Germany; <sup>8</sup>Institute of Human Genetics, Christian Albrechts University Kiel/University Hospital Schleswig-Holstein, Campus Kiel, Kiel, Germany; <sup>9</sup>Institut de Pathologie, Centre Hospitalier Universitaire Vaudois, Lausanne, Switzerland; <sup>10</sup>Institute of Pathology and <sup>11</sup>Comprehensive Cancer Center Mainfranken, University of Würzburg, Würzburg, Germany; <sup>12</sup>Department of Pathology, Massachusetts General Hospital/Harvard Medical School, Boston, MA; <sup>13</sup>Cleveland Clinic Foundation, Cleveland, OH; <sup>14</sup>Department of Pathology and Microbiology and <sup>15</sup>Division of Oncology and Hematology, Department of Internal Medicine, College of Medicine, University of Nebraska Medical Center, Omaha, NE; <sup>16</sup>Department of Laboratory Medicine and Pathobiology, Faculty of Medicine, University of Toronto, Toronto, ON, Canada; <sup>17</sup>Oslo University Hospital, Oslo, Norway; <sup>18</sup>Department of Pathology, City of Hope National Medical Center, Duarte, CA; <sup>19</sup>VU University Medical Center, Amsterdam, The Netherlands; <sup>20</sup>Hospital Universitari de Bellvitge–Institut d'Investigació Biomèdica de Bellvitge (IDIBELL), L'Hospitalet de Llobregat, Spain; <sup>21</sup>Haematological Malignancy Diagnostic Service (HMDS) Laboratory, St. James's Institute of Oncology, Leeds Teaching Hospitals NHS Trust, Leeds, United Kingdom; <sup>22</sup>Department of Pathology, School of Medicine, University of Pittsburgh, Pittsburgh, PA; <sup>23</sup>Joint Barcelona Supercomputing Center (BSC)–Centre for Genomic Regulation (CRG)–Institute for Research in Biomedicine (IRB) Research Programme in Computational Biology, Barcelona, Spain; <sup>24</sup>Institució Catalana de Recerca i Estudis Avançats (ICREA), Barcelona, Spain; <sup>25</sup>Centre Nacional d'Anàlisi Genòmica (CNAG)–CRG, Barcelona, Spain; <sup>26</sup>Laboratori de Citogenètica Molecular, Servei de Patologia, Hospital del Mar, Barcelona, Spain; <sup>27</sup>Grup de Recerca Translacional en Neoplàsies Hematològiques, Cancer Research Programme, Institut Hospital del Mar d'Investigacions Mèdiques (IMIM)–Hospital del Mar, Barcelona, Spain; <sup>28</sup>Hematopathology Section, Hospital Clínic de Barcelona, Barcelona, Spain; <sup>29</sup>Department of Clinical Pathology and <sup>30</sup>Dr Margarete “Fischer Bosch Institute” of Clinical Pharmacology, Robert Bosch Hospital, Stuttgart, Germany; <sup>31</sup>Institute of Pathology, Eberhard Karls University of Tübingen, Tübingen, Germany; <sup>32</sup>Laboratory of Pathology, Center for Cancer Research, National Cancer Institute, National Institutes of Health, Bethesda, MD; and <sup>33</sup>Department of Anatomic Pathology, University of Barcelona, Barcelona, Spain

## KEY POINTS

- Cryptic insertions of immunoglobulin light-chain enhancers are associated with *CCND2* and *CCND3* overexpression in cyclin D1<sup>-</sup> MCLs.
- Most cyclin D1<sup>-</sup> MCLs had *CCND2* or *CCND3* rearrangements whereas a small subset show upregulation of *CCNE1* and *CCNE2*.

Mantle cell lymphoma (MCL) is characterized by the t(11;14)(q13;q32) translocation resulting in overexpression of cyclin D1. However, a small subset of cyclin D1<sup>-</sup> MCL has been recognized, and approximately one-half of them harbor *CCND2* translocations while the primary event in cyclin D1<sup>-</sup>/D2<sup>-</sup> MCL remains elusive. To identify other potential mechanisms driving MCL pathogenesis, we investigated 56 cyclin D1<sup>-</sup>/SOX11<sup>+</sup> MCL by fluorescence in situ hybridization (FISH), whole-genome/exome sequencing, and gene-expression and copy-number arrays. FISH with break-apart probes identified *CCND2* rearrangements in 39 cases (70%) but not *CCND3* rearrangements. We analyzed 3 of these negative cases by whole-genome/exome sequencing and identified IGK (n = 2) and IGL (n = 1) enhancer hijackings near *CCND3* that were associated with cyclin D3 overexpression. By specific FISH probes, including the IGK enhancer region, we detected 10 additional cryptic IGK juxtapositions to *CCND3* (6 cases) and *CCND2* (4 cases) in MCL that overexpressed, respectively, these cyclins. A minor subset of 4 cyclin D1<sup>-</sup> MCL cases lacked cyclin D rearrangements and showed upregulation of *CCNE1* and *CCNE2*. These cases had blastoid morphology, high genomic complexity, and *CDKN2A* and *RB1* deletions. Both genomic and gene-expression profiles of cyclin D1<sup>-</sup> MCL cases were indistinguishable from cyclin D1<sup>+</sup> MCL. In conclusion, virtually all cyclin D1<sup>-</sup> MCLs carry *CCND2*/*CCND3* rearrangements with immunoglobulin genes, including a novel IGK/L enhancer hijacking mechanism. A subset of cyclin D1<sup>-</sup>/D2<sup>-</sup>/D3<sup>-</sup> MCL with aggressive features has cyclin E dysregulation. Specific FISH probes may allow the molecular identification and diagnosis of cyclin D1<sup>-</sup> MCL. (*Blood*. 2019;133(9):940-951)

## Introduction

Mantle cell lymphoma (MCL) is a mature B-cell malignancy genetically characterized by the primary translocation t(11;14)(q13;q32) found in the vast majority of cases.<sup>1-3</sup> This translocation juxtaposes the *CCND1* gene to an enhancer of the immunoglobulin heavy-chain gene (IGH) leading to constitutive cyclin D1 upregulation. Nevertheless, a small subset of MCL lacks cyclin D1 overexpression and the t(11;14) (cyclin D1<sup>-</sup> MCL).<sup>4-10</sup> These cases have similar morphology, phenotype, gene-expression profile, genomic alterations, and clinical behavior as conventional cyclin D1<sup>+</sup> MCL.<sup>5,11,12</sup> SOX11 is a transcriptional factor constantly overexpressed in most MCLs independent of the expression of cyclin D1 and, therefore, it is a useful marker to recognize cyclin D1<sup>-</sup> MCL cases.<sup>11</sup>

Interestingly, the first 6 cyclin D1<sup>-</sup> MCLs identified in the Lymphoma/Leukemia Molecular Profiling Project showed overexpression of cyclin D2 or cyclin D3, but evidence of chromosomal rearrangements affecting these loci was not found by fluorescence in situ hybridization (FISH) using break-apart probes.<sup>4</sup> However, different reports have detected occasional cyclin D1<sup>-</sup> MCL cases with high levels of cyclin D2 due to chromosomal translocations with immunoglobulin genes, that is, t(2;12)(p11;p13) [IGK/*CCND2*],<sup>6,8</sup> t(12;22)(p13;q21) [*CCND2*/IGL],<sup>7</sup> and a t(12;14)(p13;q32) [*CCND2*/IGH].<sup>9</sup> In the largest series of cases analyzed, we identified 55% cases (22 of 40) with *CCND2* rearrangement, preferentially with immunoglobulin light chains (68%), but *CCND3* rearrangement was not identified in the remaining cases using standard break-apart probes.<sup>5</sup> So far, only 1 single MCL case with *CCND3*/IGH rearrangement has been reported.<sup>8</sup>

Overall, the potential role of *CCND2* and *CCND3* translocations as alternative pathogenic mechanisms to *CCND1* rearrangement in cyclin D1<sup>-</sup> MCL is not yet fully understood because not all reports of rearrangements were coupled with expression studies of the rearranged cyclins or with SOX11 expression. To clarify the genetic mechanisms behind cyclin D1<sup>-</sup> MCL, we performed an integrative analysis including a complete FISH panel, next-generation sequencing (NGS), and gene-expression and copy-number arrays, in a large series of well-characterized cyclin D1<sup>-</sup> MCL.

## Methods

### Patients and samples

A total of 56 cyclin D1<sup>-</sup> MCL cases (28 partially investigated in previous studies)<sup>4,5</sup> were included in the current project based on (i) morphology and phenotype consistent with MCL (CD5<sup>+</sup> and CD23<sup>-</sup>), (ii) absence of cyclin D1 expression and t(11;14)(q13;q32), and (iii) SOX11 expression. The main clinicopathological and molecular features of the patients are described in Table 1. DNA/RNA extraction was performed from formalin-fixed and paraffin-embedded (FFPE) tissue blocks in 52 samples, fresh-frozen material in 7 samples, and Carnoy-fixed cells in 2 samples. The study was approved by the institutional review board of the Hospital Clinic of Barcelona.

### Cytogenetic analyses

FISH analyses were performed on FFPE tissue sections or fixed cells from cytogenetic cultures. The FISH panel used to interrogate breaks and juxtapositions of the loci *CCND2*, *CCND3*, *CCNE1*,

*CCNE2*, IGH, IGL, and IGK including both commercial and bacterial artificial chromosome (BAC)-labeled probes is detailed in supplemental Table 1 (available on the *Blood* Web site). The extraction and labeling of BAC and P1-derived artificial chromosome DNA, preparation of slides, and hybridization were performed according to standard procedures.<sup>13</sup> Each clone was first tested individually by hybridization on normal metaphases. Hybridizations were analyzed using standard fluorescence microscopes (Nikon Eclipse 50i or Zeiss) equipped with appropriate filter sets. Acquisition and processing of digital images were performed using the ISIS FISH Imaging System (MetaSystems, Altusheim, Germany). For the detection of IGK cryptic insertions, 2 overlapping BAC clones covering the IGK enhancer region were selected, labeled, and hybridized together with *CCND2*-, *CCND3*-, *CCNE1*-, or *CCNE2*-specific probes with different fluorochromes. Negative tissue controls for these FISH experiments included 1 reactive lymph node, 4 chronic lymphocytic leukemias (CLLs), 6 diffuse large B-cell lymphomas (DLBCLs), 1 follicular lymphoma, and 1 splenic marginal zone lymphoma (SMZL). To verify *CCNE2* gain, we used simultaneously *CCNE2* (8q22) and chr8 centromeric probes. Conventional cytogenetics was performed on G-banded chromosomes and results were described according to An International System for Human Cytogenomic Nomenclature (ISCN).<sup>14</sup>

### NGS analyses

Somatic structural variants (SVs) were analyzed by different NGS approaches in 5 MCL cases: long-insert-size (7-10 kb), mate-pair whole genome sequencing (MP-WGS) of 4 tumors and 10 normal unmatched DNA; paired-end whole-genome sequencing (WGS) of tumor and matched normal sample of 1 patient; and whole-exome sequencing (WES) in 3 tumors (supplemental Figure 1; supplemental Table 2).<sup>15,16</sup> Libraries were constructed according to standard protocols (Illumina), and sequencing was performed with an Illumina HiSeq 2000 instrument.<sup>15</sup> Reads were mapped to the hg19 human reference genome using the Burrows-Wheeler aligner (BWA-MEM version 0.7.5a-r405). Polymerase chain reaction (PCR) duplicates were removed using the MarkDuplicates algorithm from Picard tools. SVs were analyzed using different pipelines: (i) BWA with the "samse" option was used for MP-WGS analysis in combination with custom scripts to detect interchromosomal translocations supported by at least 4 reads, followed by visual inspection (ID3, ID6, ID73, and ID76), (ii) Smufin<sup>17</sup> and Lumpy<sup>18</sup> were used to detect SVs in the WGS of case ID73, and (iii) custom scripts were used to analyze/confirm potential interchromosomal SVs in the WES data (ID3, ID5, and ID6). We excluded SVs in repetitive or ambiguously aligned regions in the MP-WGS analysis. Due to the lack of germline DNA for most samples, SVs present both in 2 or more of the 4 MP-WGS and 1 or more of 10 normal samples or present in dbVar were removed as potential germline variants/artifacts. In case ID73, copy-number alterations (CNAs) from WGS were analyzed using FREEC<sup>19</sup> and ASCAT algorithms, whereas single-nucleotide variants and indels were analyzed using 3 different pipelines: Smufin,<sup>17</sup> Sidrón,<sup>20</sup> and Mutect2,<sup>21</sup> and annotated by Annotvar. Verification of break-points (supplemental Table 3) and mutations was performed by Sanger sequencing.

### Gene-expression and copy-number analyses

Total RNA from 14 cyclin D1<sup>-</sup> MCLs and 7 cyclin D1<sup>+</sup> MCLs was extracted from FFPE tissue biopsies, processed using SensationPlus FFPE Amplification and the 3' IVT Labeling

**Table 1. Clinicopathological and molecular features of the 56 cyclin D1<sup>-</sup> MCLs**

Parameter	Total, n = 56	Cyclin D2 <sup>+</sup> , n = 43	Cyclin D3 <sup>+</sup> , n = 9	Cyclin E <sup>+</sup> , n = 4	P
Median age, y	65	66	60	75	.161
Ratio male/female	2.4/1	3.2/1	2/1	0/1	.029*
<b>Growth pattern (%)</b>					1
Nodular and/or diffuse	50/52 (96)	40/42 (95)	6/6 (100)	4/4 (100)	
Mantle zone	2/52 (4)	2/42 (5)	0/6 (0)	0/4 (0)	
<b>Morphology (%)</b>					.029*
Classical	43 (81)	34/40 (85)	8/9 (89)	1/4 (25)	
Blastoid	10 (19)	6/40 (15)	1/9 (11)	3/4 (75)	
<b>Expression (%)</b>					
SOX11 <sup>+</sup>	56 (100)	43/43 (100)	9/9 (100)	4/4 (100)	1
CD5 <sup>+</sup>	54/55 (98)	43/43 (100)	7/8 (88)	4/4 (100)	.218
CD23 <sup>-</sup>	47/47 (100)	36/36 (100)	7/7 (100)	4/4 (100)	1
CD10 <sup>-</sup>	39/39 (100)	31/31 (100)	4/4 (100)	4/4 (100)	1
Ig λ light-chain restriction	20/25 (80)	15/19 (79)	3/3 (100)	2/3 (67)	1
Ki67 (≥30%)	24/42 (57)	18/33 (55)	2/5 (40)	4/4 (100)	.153
<b>Median expression (qPCR)</b>					
CCND2	17.0	124.8	7.0	4.8	<.001*
CCND3	2.0	1.8	18.9	2.6	<.001*
CCNE1	1.0	1.1	0.9	7.6	.009*
CCNE2	0.8	0.8	0.6	3.8	.077
<b>Molecular</b>					
Median CNA per case	10	9	9	17	.098
Chromothripsis (%)	10/42 (24)	6/29 (21)	3/9 (33)	1/4 (25)	.847
-17p13/TP53 (%)	8/42 (19)	8/29 (28)	0/9 (0)	0/4 (0)	.144
-11q22/ATM (%)	14/42 (33)	9/29 (31)	5/9 (55)	0/4 (0)	.140
-9p21/CDKN2A (%)	20/42 (48)	14/29 (48)	2/9 (22)	4/4 (100)	.033*
-13q14/RB1 (%)	17/42 (40)	9/29 (31)	4/9 (44)	4/4 (100)	.030*
+18q (%)	15/42 (36)	8/29 (28)	3/9 (33)	4/4 (100)	.025*
+3q (%)	23/42 (55)	18/29 (62)	3/9 (33)	2/4 (50)	.378
-1p (%)	16/42 (38)	10/29 (34)	6/9 (67)	0/4 (0)	.049*
<b>Clinical data (%)</b>					
Treated at diagnosis†	38/41 (93)	27/29 (93)	7/8 (88)	4/4 (100)	.589
High-dose therapy	2/41 (5)	2/29 (7)	—	—	
Immunochemotherapy	25/41 (61)	18/29 (62)	3/8 (38)	4/4 (100)	
Other	11/41 (27)	7/29 (24)	4/8 (50)	—	
Observation	3/41 (7)	2/29 (7)	1/8 (13)	—	
3-y overall survival, % (95% CI)	68 (54-86)	59 (42-83)	100 (100-100)	75 (43-100)	.424

—, no cases; CI, confidence interval; Ig, immunoglobulin.

\*P < .05 was considered significant. P values were calculated using the Fisher's exact and Kruskal-Wallis tests for categorical or continuous variables between the 3 groups, respectively.

†High-dose therapy includes cytarabine-based immunochemotherapy; immunochemotherapy includes rituximab plus cyclophosphamide, doxorubicin, vincristine, and prednisone (R-CHOP) and R-CHOP-like regimens; and other includes low-dose therapy (alkylating agents alone or in combination) and radiotherapy.

Kit, and hybridized on GeneChip Human Genome U133 Plus 2.0 arrays (Thermo Fisher Scientific, Waltham, MA). Arrays were washed and stained using GeneChip Fluidics Station 450 (Thermo Fisher Scientific) and GeneChip Scanner. Limma<sup>22</sup> was used to detect differentially expressed probe sets, and P values were adjusted by the Benjamini-Hochberg method. In 38 cyclin D1<sup>-</sup> MCLs, 4 CLLs, and 16 normal samples, gene-expression levels of *CCND2*, *CCND3*, *CCNE1*, and *CCNE2* were investigated by quantitative PCR (qPCR) as previously

described,<sup>5</sup> using *GUSB* as endogenous control and Universal Human Reference RNA as a calibrator (supplemental Tables 2 and 4). qPCR for *CCNE1* and *CCNE2* was also analyzed in 3 blastoid MCLs, 6 DLBCLs, and 7 SMZLs. Cyclin E1 protein expression was analyzed by immunohistochemistry (antibody clone sc-247, dilution 1/100; Santa Cruz Biotechnology) in 12 cyclin D1<sup>-</sup> MCLs, 1 CLL, 2 SMZLs, and in control tissues (testis as positive control and tonsil and reactive lymph node as negative controls). CNAs were evaluated in 42 cyclin D1<sup>-</sup> cases

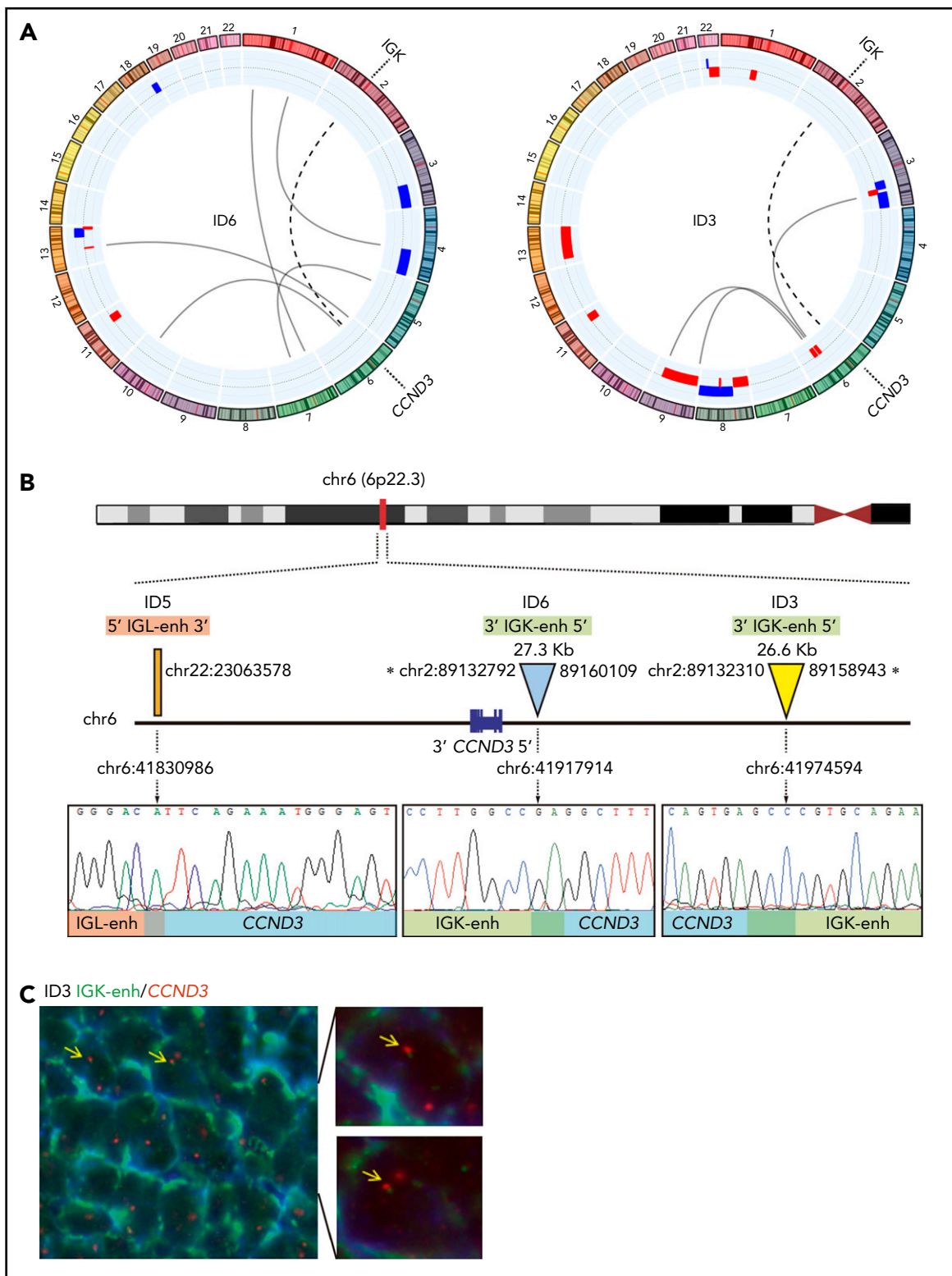


**Figure 1. Cryptic insertions of immunoglobulin light-chain enhancer regions near the *CCND3* gene in 3 cyclin D1-MCL.** (A) Circos plots with interchromosomal SVs detected by MP-WGS (black lines) and CNA detected by copy-number arrays (blue for gains and red for losses) in cases ID6 and ID3. The rearrangement between chr2 (IGK-enh) and chr6 (*CCND3*) in both cases is indicated with a discontinuous line. (B) Schematic representation of the 6p region around the *CCND3* locus showing the location of the cryptic insertion of the IGK-enh (chr2) close to 5' of the *CCND3* gene in cases ID6 and ID3 (the length of the inserted fragments is indicated), and the location of the cryptic insertion of the IGL enhancer (chr22) near 3' of the *CCND3* gene in case ID5. The breakpoints were detected by MP-WGS (cases ID3 and ID6), and WES (case ID5), and further verified and refined to base pair resolution by Sanger sequencing in the 3 cases. There were 1-, 2-, and 3-bp homology at the breakpoint junctions, respectively. (C) Verification of the cryptic IGK/*CCND3* insertion by FISH in case ID3 using the fusion probe IGK-enh (labeled in green) with *CCND3* (labeled in red). FISH analysis shows 2 red and 2 green signals in normal cells and the yellow arrows highlight cells with 1 red and 1 small green signal juxtaposed, indicating the presence of the IGK insertion. Magnifications of cells with the rearrangement are shown at the right side (4',6-diamidino-2-phenylindole [DAPI] stain; original magnification  $\times 100$ ). \*Breakpoints estimated from MP-WGS data. enh, enhancer.

(47 samples) with different approaches including: CGH-array Agilent 1M (Agilent, Santa Clara, CA), and single-nucleotide polymorphism (SNP) arrays 500K, SNP6.0, or Oncoscan CNV (Thermo Fisher Scientific) (supplemental Table 2). CNA analysis was performed using Nexus Biodiscovery version 9.0 software (Biodiscovery, Hawthorne, CA) as previously described.<sup>5,16</sup> All cases were visually inspected by at least 2 independent observers.

## Results

### Identification of cryptic rearrangements of IGK and IGL enhancer regions and cyclin D genes in cyclin D1<sup>-</sup> MCL

To understand the molecular alterations present in cyclin D1<sup>-</sup> MCL cases, we initially performed FISH analysis using *CCND2*, *IGH*, *IGK*, and *IGL* break-apart probes in 56 cyclin D1<sup>-</sup> MCLs and identified 39 cases (70%) with *CCND2* rearrangements (cyclin D2<sup>+</sup> MCL), preferentially involving light chains *IGK* (55%) and *IGL* (13%) (supplemental Figure 1). The remaining 17 patients (30%) without *CCND2* rearrangements were analyzed using a *CCND3* break-apart FISH probe but none of them showed rearrangements. Detailed FISH results of all cases are listed in supplemental Table 5.

To investigate the presence of potential rearrangements that might have been undetectable by standard FISH approaches, we performed MP-WGS in 2 cases that were negative for FISH rearrangements of *CCND2* and *CCND3* (ID3 and ID6). We detected several somatic interchromosomal SVs (4 in ID3 and 6 in ID6) (Figure 1A; supplemental Table 6). Strikingly, both cases showed a similar rearrangement involving *IGK* in chromosome 2 and *CCND3* in chromosome 6, which consisted of a small insertion (26.6 kb for ID3 and 27.3 kb for ID6) including the *IGK* enhancer. Virtually the entire *IGK* enhancer (26.4 kb), as defined by chromatin states in normal mature B cells,<sup>23</sup> was integrated upstream of the *CCND3* gene (8.4 kb upstream in case ID6 and 65 kb in case ID3). The allelic fraction of the alterations was ~41% to 44%, suggesting that they were present in virtually all tumor cells. We confirmed these cryptic insertions by Sanger sequencing in both cases and we could identify the breakpoint at single-nucleotide resolution (Figure 1B). This insertion was also observed by WES in case ID6. In addition, we validated these findings by FISH in case ID3 using a new combination of fusion probes, 1 covering the *CCND3* gene and the other including the enhancer of *IGK* (*IGK*-enh) (Figure 1C). Additionally, WES analysis of case ID5 (also negative for FISH with *CCND3* break-apart probe) revealed a similar cryptic insertion of the *IGL* enhancer region in chromosome 22 near 3' of the *CCND3* gene, which was further verified by Sanger sequencing (Figure 1B). Interestingly, those 3 cases (ID3, ID5, and ID6) in which we identified the cryptic *IGK/L* enhancer and *CCND3* rearrangement (enhancer hijacking) were initially reported to have cyclin D3 overexpression by microarray-expression analysis,<sup>4</sup> highlighting the functional impact of the cryptic rearrangement at the messenger RNA (mRNA) level, and the potential utility of cyclin D2/D3 expression to help to identify these tumors with cryptic rearrangements in the absence of conventional translocation of the cyclins.

In addition, we performed MP-WGS of case ID76, positive for the *IGK/CCND2* rearrangement by FISH and also by karyotype. We detected 23 interchromosomal SVs, including 2 that confirmed the *IGK/CCND2* reciprocal translocation. Interestingly, the MP-WGS

coupled with SNP6.0 array data allowed for refinement of several alterations of the karyotype (Figure 2; supplemental Table 6).

### Identification of additional cryptic *IGK/CCND3* and *IGK/CCND2* by FISH

The finding of this enhancer-hijacking phenomenon in cyclin D1<sup>-</sup> MCL associated with *CCND3* overexpression prompted us to explore the expression of all cyclins of the G1 phase of the cell cycle (*CCND2*, *CCND3*, *CCNE1*, and *CCNE2*) in cyclin D1<sup>-</sup> MCL, CLL, and nonneoplastic samples (reactive lymph nodes and tonsils) by qPCR. As expected, all *CCND2*-rearranged cases tested ( $n = 24$ ) (cyclin D2<sup>+</sup> MCL) showed elevated levels of *CCND2* (median *CCND2* expression = 127.5) compared with nonrearranged *CCND2* MCL cases (median, 7.0) ( $P < .001$ ) (Figure 3). Interestingly, among the 14 cases tested without *CCND2* or *CCND3* rearrangements, 6 cases overexpressed *CCND3* (median 18.9), 4 cases overexpressed *CCND2* (median 66.2), and the remaining 4 cases overexpressed concomitantly *CCNE1* along with *CCNE2* (median, 7.6 and 3.8, respectively) (Table 1; Figure 3; supplemental Figure 1).

Given the high levels of *CCND3* in these additional 6 cyclin D1<sup>-</sup> MCL cases, we explored the presence of similar cryptic *IGK* and *CCND3* juxtapositions by FISH using the *IGK*-enh and *CCND3* fusion probe. We detected fusion *IGK/CCND3* signals in all 6 cases (supplemental Figure 2A; supplemental Table 5), but not in any of the 9 control samples tested. The presence of these cryptic immunoglobulin insertions near the *CCND3* gene leading to *CCND3* overexpression prompted us to hypothesize that the remaining 4 cases with high levels of *CCND2* expression (and negative for *CCND2* breaks using break-apart FISH probes) could present similar cryptic aberrations. Thus, we performed FISH using *IGK*-enh and *CCND2* probes and we could detect the juxtaposition of both signals in all 4 cases (supplemental Figure 2B-C; supplemental Table 5), but not in the 9 controls tested. Together, these data show that 13 of the 17 (76%) MCLs negative for *CCND2/D3* rearrangements using break-apart probes had *IGK/L* enhancer hijacking into either *CCND3* (9 cases) or *CCND2* (4 cases).

### Absence of detectable primary genetic events in a small subset of cyclin D1<sup>-</sup> MCL

After the identification of the cryptic *IGK* enhancer rearrangements with *CCND3* and *CCND2* in MCLs negative for the *CCND2/D3* break-apart by FISH, only 4 of the 56 cyclin D1<sup>-</sup> MCLs remained without an identified primary genetic event. All 4 cases overexpressed concomitantly *CCNE1* and *CCNE2* mRNA but not the remaining cyclin D genes. We performed cyclin E1 immunohistochemistry and the 3 cases tested (ID26, ID73, and ID77) were strongly positive in most of the cells (>65%) (Figure 4A) as compared with only 1 of 9 cyclin D2<sup>+</sup> or cyclin D3<sup>+</sup> MCLs, 1 of 3 B-cell lymphomas (a SMZL sample), and none of the 2 nonmalignant lymphoid tissues tested. These findings confirmed the cyclin E1 overexpression also at the protein level in these cases. We also compared the *CCNE1/E2* mRNA expression in 3 cyclin D1<sup>+</sup> blastoid MCLs, 6 DLBCLs, and 7 SMZLs. *CCNE1/E2* levels were high in the 4 cyclin E<sup>+</sup> MCLs but were negative or undetectable in the other cases (supplemental Figure 3). To determine whether the *CCNE* overexpression could be due to a genomic rearrangement, we performed FISH using a break-apart probe and the *IGK* enhancer with *CCNE1* or *CCNE2* probes in 3 cases but all were negative. Furthermore, these cases showed

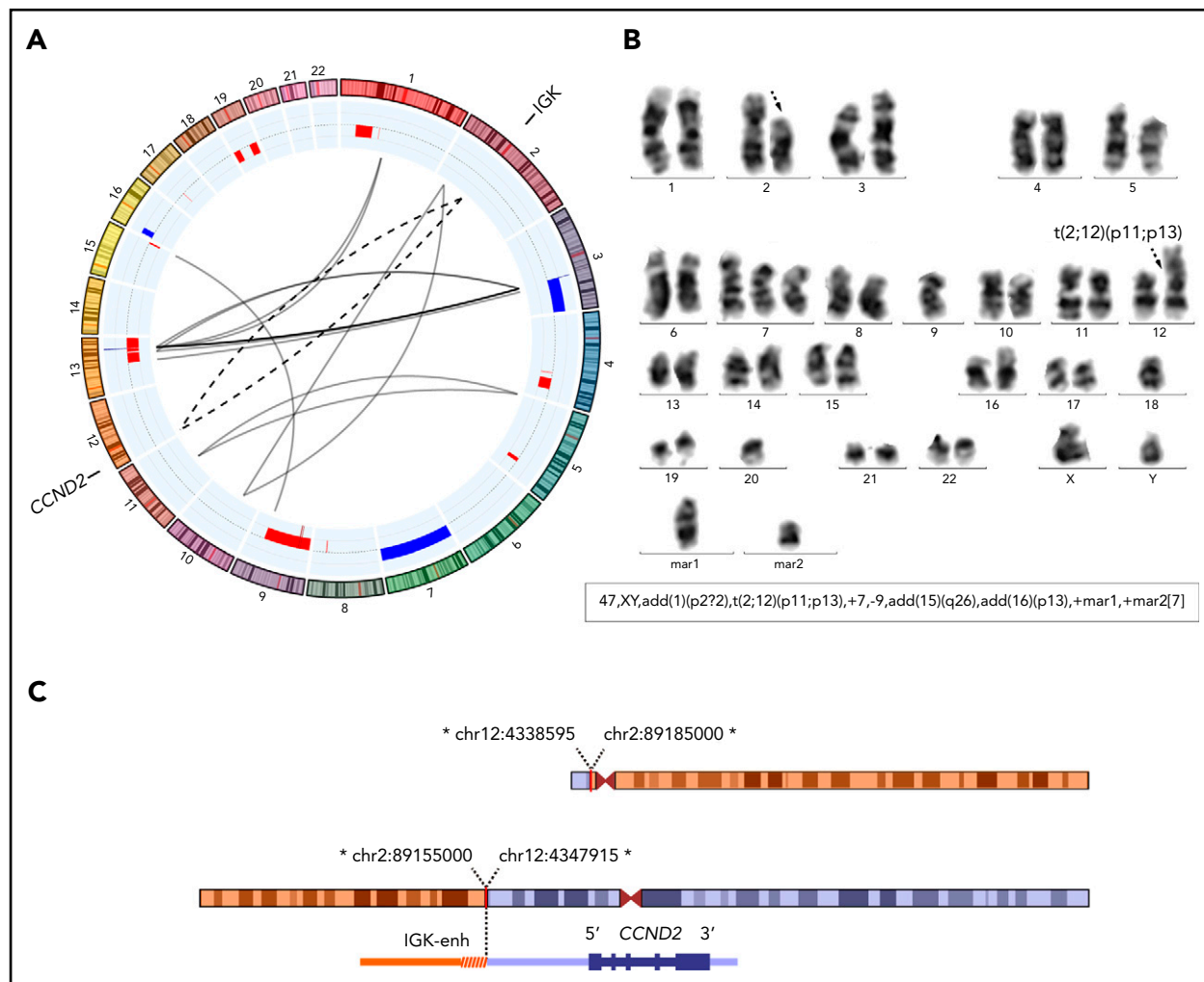


**Figure 2. Conventional *CCND2* rearrangement in a cyclin D2<sup>+</sup> MCL.** (A) Circos plot with interchromosomal SVs detected by MP-WGS (black lines) and CNA detected by copy-number arrays (blue for gains and red for losses) in case ID76. The conventional IGK/*CCND2* reciprocal translocation is indicated with 2 discontinuous lines for both derivative chromosomes. Among other SV, 12 clustered rearrangements were found between chromosomes 3 and 13 (at both regions of high copy gain). (B) A representative metaphase and the karyotype with the IGK/*CCND2* rearrangement (black discontinuous arrows) and other numerical and structural aberrations concordant with the results of MP-WGS and copy-number array: trisomy 7; loss of chromosome 9; and 2 marker chromosomes consistent with some of the rearranged chromosomes. (C) Schematic representation of the derivative chromosomes resulting from the translocation and zoomed image of *CCND2* locus. \*All breakpoints were estimated from MP-WGS analysis (chr2 in orange, containing the IGK enhancer and chr12 in blue containing the *CCND2* gene).

no evidence of IGK, IGL, and IGH rearrangement by FISH (supplemental Table 5).

We then performed MP-WGS (tumor) and WGS (tumor and normal) of the remaining case with *CCNE1/E2* overexpression (case ID73) (Figure 4B; supplemental Table 7). We could not find any genetic rearrangement involving immunoglobulin, cyclin D, or cyclin E genes. Of note, we detected a 8q21.2-q23 high-level gain (~6 copies estimated by WGS), which included the *CCNE2* locus and was confirmed by FISH (Figure 4C-D), and 2 homozygous deletions, 1 truncating *RB1* at 13q14 and 1 affecting *CDKN2A* at 9p21. We also detected 32 intrachromosomal and 35 interchromosomal rearrangements, 12 of them only detected by MP-WGS. Finally, we analyzed the genes truncated by SVs and found disruption of 50 genes, including cancer-associated genes such as *NBN*, *BCL2L11* (*BIM*), and *ARID1B* among others. We detected 31 somatic protein-coding mutations by WGS analysis, none of them previously reported in MCL samples (Figure 4B; supplemental Table 8).<sup>16,24</sup>

### Global expression, genomic profiles, and overall survival in cyclin D1<sup>-</sup> MCL

We compared the global gene-expression profile of 14 cyclin D1<sup>-</sup> MCLs and 7 cyclin D1<sup>+</sup> MCLs. The unsupervised clustering analysis did not segregate these cases into different clusters. Moreover, principal component analysis showed that the main source of variability (45%) was not related to the absence of cyclin D1 expression. *CCND1* was the only significant differentially expressed gene (adjusted  $P = 2.3 \times 10^{-11}$ ), and besides overexpression of *CCND2* (10 cases), *CCND3* (1 case), or concomitant *CCNE1/CCNE2* (2 cases), no other overexpressed genes were found (supplemental Figure 4).

We compared the global profile of CNA of 42 cyclin D1<sup>-</sup> MCLs with 116 previously published cyclin D1<sup>+</sup>/SOX11<sup>+</sup> MCLs<sup>12,16,25</sup> and the profiles were indistinguishable. Similar to cyclin D1<sup>+</sup> MCL, cyclin D1<sup>-</sup> MCL had a high complex profile (median 10 CNAs per case), and frequent deletions of 9p21/*CDKN2A* (48%), 11q22/*ATM* (33%),

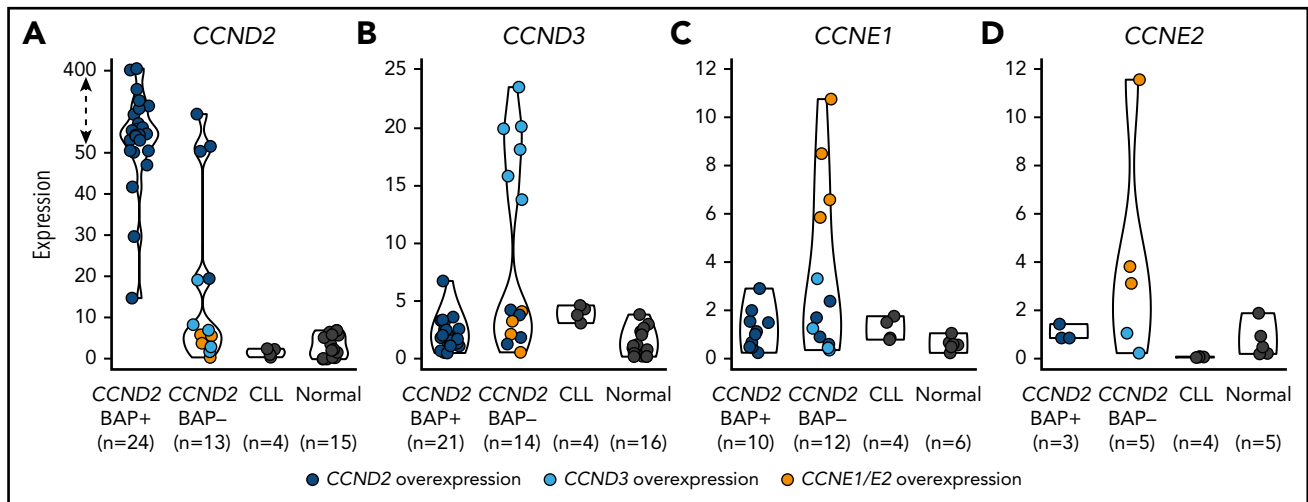


**Figure 3. Expression of G1-phase cyclins by qPCR.** The expression of (A) *CCND2*, (B) *CCND3*, (C) *CCNE1*, and (D) *CCNE2* was represented according to 4 categories: MCL positive or negative for the *CCND2* break-apart FISH test (*CCND2* BAP<sup>+</sup> and *CCND2* BAP<sup>-</sup>, respectively), CLL, and nonneoplastic lymphoid samples (normal). Colored dots highlight cases with overexpression of *CCND2* (dark blue), *CCND3* (light blue), *CCNE1/CCNE2* (orange). The overexpression cutoff values were calculated as the mean plus 3 standard deviations in nonrearranged cases: 15.1 for *CCND2*, 6.2 for *CCND3*, 3 for *CCNE1*, and 2.4 for *CCNE2*. The y-axis of the *CCND2* graph has been transformed for the expression values above 50 (dashed arrow).

and 17p13/*TP53* (19%) (Table 1; Figure 5; supplemental Figure 5A; supplemental Table 9). No statistical differences were found between cyclin D2<sup>+</sup> (n = 29) vs cyclin D3<sup>+</sup> (n = 9) MCL subgroups (supplemental Figure 5B). Interestingly, all 4 cases with *CCNE1/E2* overexpression showed alterations in cell cycle and apoptosis-related genes, such as focal homozygous deletions of 9p21 (*CDKN2A*), 13q14 deletions (*RB1*), and large high-copy gains of 18q (*BCL2*). These 4 cases also had a higher number of CNAs (median, 17 CNAs per case) than cyclin D2<sup>+</sup> or cyclin D3<sup>+</sup> MCLs (median 9 CNA/case) (Table 1). We also analyzed the CNAs of 2 different tumor samples of the same patient in 5 cases (1 synchronous and 4 sequential) and they showed both common and unique alterations, suggesting the presence of genetically heterogeneous subpopulations and clonal evolution in each case (supplemental Figure 5C).

The cyclin D1<sup>-</sup> MCL patients had overall survival similar to cyclin D1<sup>+</sup>/*SOX11*<sup>+</sup> MCL (supplemental Figure 6A).<sup>26</sup> It is noteworthy that although the 3-year overall survival was higher in patients with cyclin D3<sup>+</sup> than in patients with cyclin D2<sup>+</sup> or cyclin E<sup>+</sup> (100%, 59%, and 75%, respectively), these differences were not statistically significant (Table 1; supplemental Figure 6B).

## Discussion

MCL is a well-characterized lymphoid neoplasm with the t(11;14) leading to cyclin D1 overexpression as the primary genetic event. However, a particular subset of cases with the same histology and phenotype but lacking cyclin D1 expression has been recognized.<sup>1</sup> We previously reported chromosomal translocations of the *CCND2* locus with immunoglobulin genes in approximately one-half of these cases and emphasized the value of this approach for the recognition of a proportion of cyclin D1<sup>-</sup> MCL.<sup>5</sup> Nevertheless, the primary rearrangement in the remaining cases could not be established. We document here a deep comprehensive analysis of the largest series of

cyclin D1<sup>-</sup> MCL cases ever reported, integrating molecular and genetic data with NGS technologies, which allowed us to unveil for the first time selective cryptic insertions of *IGK/L* enhancer regions (enhancer hijacking) into cyclin D genes in the majority of the cases that lacked a *CCND2* conventional rearrangement.

Our integrative study found that 16% of cyclin D1<sup>-</sup> MCLs had *CCND3* rearrangements, all of them consisting of a cryptic insertion of the *IGK/L* enhancer that was associated with *CCND3* overexpression and may be considered an alternative molecular mechanism to *CCND1* or *CCND2* primary translocations. Interestingly, a *CCND3/IGH* translocation has been previously reported in 1 MCL,<sup>8</sup> 1 low-grade B-cell lymphoma, 3 splenic lymphomas, and 7 aggressive B-cell lymphomas.<sup>27-30</sup> Notably, in all of these cases, the *CCND3* rearrangement was with *IGH* and detectable by conventional cytogenetics. Intriguingly, some of these cases expressed CD5, and had blastoid morphology and unmutated *IGHV* with splenic and leukemic involvement. Although *SOX11* expression was not studied, these features suggest that at least some of these cases could correspond to MCL. In multiple myeloma, 15% to 25% cases have *CCND1/IGH* rearrangement or *CCND1* gain/amplification coupled with *CCND1* overexpression, 3% to 5% have *CCND3/IGH* rearrangement associated with *CCND3* overexpression, whereas *CCND2* overexpression has been detected in a subset of 5% cases without apparent genomic alterations.<sup>31,32</sup> Interestingly, no *CCND3* rearrangement with *IGK* has been previously detected in human lymphomas, but the application of RNA-sequencing analyses of a canine DLBCL showed the presence of an *IGK/CCND3* rearrangement associated with overexpression of *CCND3*.<sup>33</sup>

In our series, a large proportion of cyclin D1<sup>-</sup> MCL had conventional *CCND2* rearrangements (70%), a higher frequency than previously reported (55%).<sup>5</sup> We have now identified an

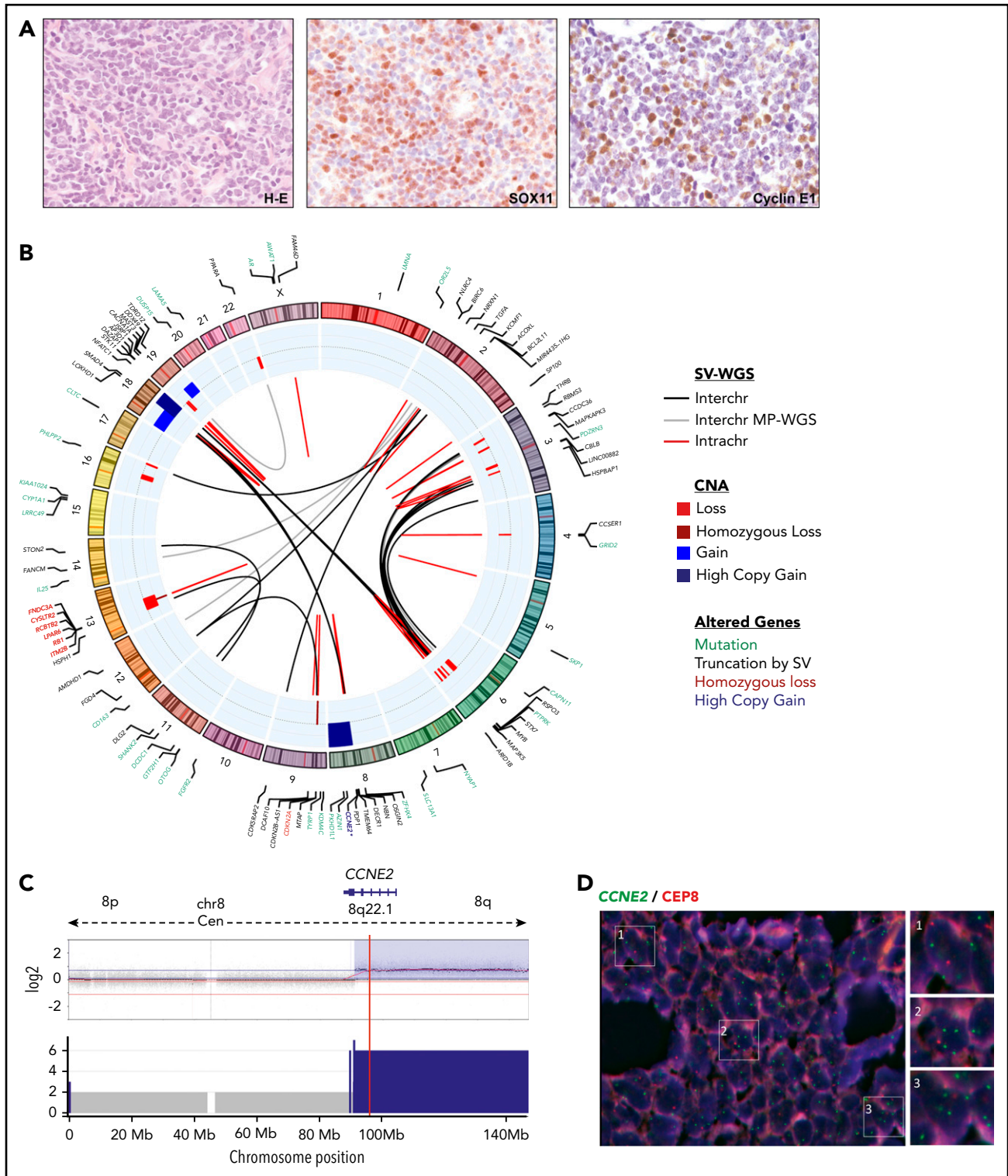


**Figure 4. Comprehensive genetic characterization of an MCL for *CCND1*, *CCND2*, and *CCND3* (*ID73*).** (A) Tumor cells from the skin lesion had a blastoid morphology (hematoxylin and eosin [H-E] stain; original magnification  $\times 40$ ), nuclear positivity for SOX11 ( $\times 40$ ), and cyclin E1 ( $\times 40$ ). (B) Circos plot representing, from inner to outer circles: SVs detected by WGS (black lines for interchromosomal and red for intrachromosomal rearrangements) or detected only by MP-WGS (gray lines); CNAs are represented in blue (gains and high copy gains) and red (losses and homozygous losses) palettes. In the outer circle are the genes altered by mutations (green), genes disrupted by SVs (black), genes affected by homozygous deletions (red), and the *CCNE2* gene with high-level gain (dark blue). No rearrangements of any cyclin or immunoglobulin genes could be detected. There were 2 dense clusters of interchromosomal rearrangements: (i) 1 between chromosomes 3 and 6, at the regions of copy-number loss; and (ii) between chromosomes 8 and 18 at the regions of high copy gain. The gain of chromosome 19 and the loss of chromosome 22 were also supported as a reciprocal rearrangement by MP-WGS. The tumor purity of the case inferred by ASCAT was 78.2% and the ploidy 2.13 (diploid). (C) Chromosome 8 profile showing a partial 8q high-level gain (including the *CCNE2* gene locus, indicated by the red line) by 2 different techniques; SNP6.0 copy-number arrays (top) and WGS analysis (bottom). (D) FISH with a locus-specific *CCNE2* probe (green) and a centromeric chromosome 8 probe (orange) confirming that most tumors cells had at least 2 extra copies of the *CCNE2* gene. Magnifications of 3 regions with the gain were shown at the right side (DAPI stain; original magnification  $\times 100$ ).



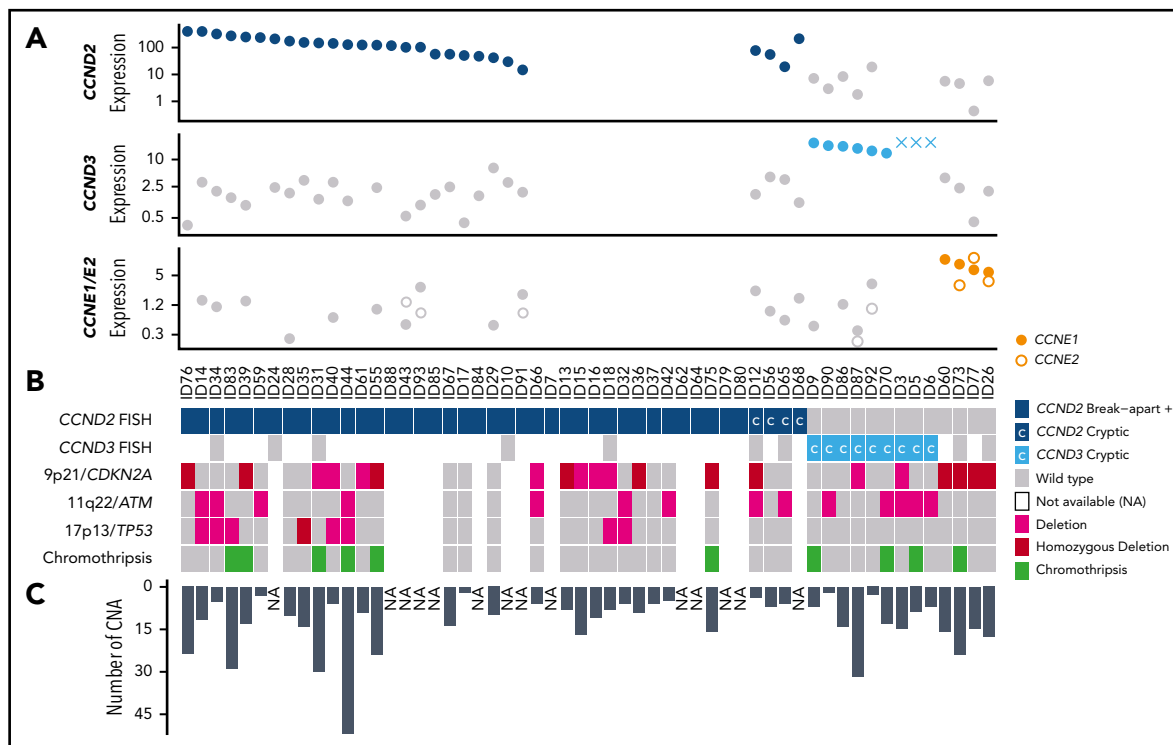


**Figure 5. Global genetic landscape of the 56 cyclin D1-MCL.** Each MCL case is represented in a column and several specific molecular analysis in different rows. From top to bottom: (A) 3 plots showing cyclin-expression levels detected by qPCR (and by gene-expression arrays in 3 cases, indicated with "X"); (B) FISH results using break-apart or specific IGK-enh and *CCND2* or *CCND3* probes to detect cryptic rearrangements (rearranged cases in dark and light blue, respectively, and cryptic rearrangements are indicated with "C"); deletions of 9p21, 11q22, and 17p13 by copy-number arrays (deletion in pink, homozygous deletion in bordeaux); and presence of chromothripsis (green). (C) The bar graph indicates the number of CNAs detected in each case. NA, not available.

additional subset of 7% cases with cryptic IGK/*CCND2*. Interestingly, *CCND2* is preferentially rearranged with immunoglobulin light-chain genes instead of IGH, IGK being more frequent than IGL (83% and 17%). Similarly, 8 *CCND3* rearrangements were with IGK, only 1 with IGL, and none with IGH. Of note, both *CCND2* and *CCND3* chromosomal breaks occur in a large region (including the 5' or 3' of *CCND3*) whereas the IGK breaks occur in a restricted region that contained the enhancer element.

One of the most remarkable findings in our study was the restricted small insertion of the IGK/L enhancer close to the *CCND2/D3* genes associated with their respective overexpression, a finding not previously detected in lymphoid neoplasms. We could resolve the breakpoints at single-nucleotide resolution identifying 1 to 3 identical nucleotides on both sides of the breakpoints. These special enhancer rearrangements seem to parallel the mechanism of enhancer hijacking activating known oncogenes recently identified in solid tumors and some lymphoid neoplasms. In solid tumors, recurrent SVs bring together a distal active enhancer to an oncogene promoting its expression. This mechanism has been identified for *MYC* and *MYCN* in high-risk pediatric neuroblastoma<sup>34</sup>; *TERT* in neuroblastoma<sup>35</sup>; *PRDM6*<sup>36</sup>; *GFI1*, *GFI1B*, and *DDX31*<sup>37,38</sup> in medulloblastoma; and *IGF2* in colorectal cancer.<sup>39</sup> *MYC* rearrangements with superenhancers from nonimmunoglobulin genes (ie, *NSMCE2*, *TXNDC5*, *FAM46C*, *FOXO3*, *PRDM1*) have been frequently found in multiple myeloma.<sup>40</sup> In addition to translocations, lymphoid neoplasms may have other small-scale SVs involving active enhancers such as amplifications of enhancer regions close to oncogenes or selective deletions and inversions that reposition candidate

enhancer elements in the vicinity of oncogenes.<sup>41,42</sup> All of these findings emphasize that SVs targeting active enhancer regions may be a mechanism of activating oncogenes more prevalent than initially thought and present across different cancer types. It would be interesting to explore whether the "immunoglobulin enhancer insertions" also affect other oncogenes such as *MYC*, *BCL2*, or *CCND1* and functionally confirm the effect of these insertions on gene overexpression in B-cell lymphomas with high mRNA or protein expression but not carrying the canonical translocations.

In the present study, we demonstrated that 93% of cyclin D1-MCLs have *CCND2* or *CCND3* rearrangements. However, a small number of cases ( $n = 4$ ), representing 7% of cyclin D1-MCLs, lacked a genetic alteration and overexpression of these cyclins, despite having the morphology and phenotype of MCL. In this minority of cases, we observed overexpression of *CCNE1* and *CCNE2* but without a primary structural rearrangement. The expression levels of these cyclins, although significantly higher than in other MCL and controls, were relatively moderate, not suggestive of being triggered by a translocation. In addition, all 4 cases showed concomitantly similar levels of both *CCNE1* and *CCNE2* genes, located in different chromosomes. The mechanism/s leading to their concomitant upregulation in these cases are unclear. Only one of the cases had a high-copy gain of *CCNE2* gene (at 8q22.1) but no concomitant gain of *CCNE1* (at 19q12), and these 2 genomic regions were not gained/amplified in the remaining 3 cases. A potential explanation could be that these cases may have an upstream common dysregulation mechanism. In contrast to cyclin D genes, the rearrangement of *CCNE1* in B-cell

neoplasms is exceptionally rare with only a single reported case of DLBCL with IGH/CCNE1 rearrangement and cyclin E1 protein overexpression.<sup>43</sup> Another feature of the 4 cyclin E<sup>+</sup> MCLs was a high genomic complexity, which is in line with previously reported CCNE1 dysregulation (by locus amplification and/or overexpression) in solid tumors, associated with chromosome instability and aggressive behavior,<sup>44-47</sup> and worse prognosis in DLBCL.<sup>48</sup> The lack of overexpression of classic cyclin Ds in these 4 cases may make their classification as MCL debatable. The main differential diagnosis may be DLBCL with CCNE overexpression.<sup>48</sup> However, SOX11 expression has only been detected in 1 of 339 DLBCLs investigated in 5 previous studies.<sup>49-53</sup> Therefore, the very rare expression of SOX11 in DLBCL and the common expression of SOX11 in MCL together with the classic or blastoid MCL morphology, CD5 expression, and the aggressive clinical course in our cases favor the closer relationship of these CCNE<sup>+</sup> cases with MCL rather than DLBCL. Further studies are needed to confirm the most appropriate taxonomy of these uncommon cases.

Overall, we show that cyclin D1<sup>-</sup> and cyclin D1<sup>+</sup> MCL share a common expression and genomic profile as well as clinical outcome.<sup>26,54</sup> Our results highlight that CCND2, CCND3, and possibly also CCNE1/E2, may be bona fide alternative alterations to CCND1 in MCL pathogenesis, which, together with SOX11 overexpression, may represent the main initial hits in MCL.<sup>55</sup> These findings may also have diagnostic implications. The identification of CCND2/D3 translocations with immunoglobulin genes in virtually all cyclin D1<sup>-</sup> MCLs confirms that the morphology and phenotype combined with SOX11 positivity are appropriate to recognize these tumors. The study of CCND2/D3 translocations described here may be useful in the differential diagnosis of tumors with blastoid or pleomorphic morphology because lymphoblastic lymphomas may express SOX11.<sup>11,49</sup> The finding of these translocations or very high CCND2/D3/E1/E2 mRNA levels would favor the diagnosis of MCL. CCNE1/E2 overexpression was associated with blastoid morphology, high genomic complexity, high proliferation, and short survival, consistent with the role of these cyclins as potent oncogenes.<sup>44</sup>

In conclusion, using an integrative molecular and genetic analysis, we have identified immunoglobulin light-chain enhancer hijacking next to CCND2 or CCND3 genes in 23% of cyclin D1<sup>-</sup> MCLs. We also recognized a small subset of aggressive cyclin D1<sup>-</sup> MCLs carrying cyclin E dysregulation. In addition to the pathogenic significance of these findings, the approach used here may be useful for the diagnosis of these tumors.

## Acknowledgments

The authors thank the Hematopathology Collection for sample procurement; Silvia Martín, Noelia García, Candida Gómez, Cristina Capdevila, and María Rodríguez-Rivera for excellent technical assistance; the Molecular Cytogenetic Platform of IMIM, Hospital del Mar (Barcelona) for providing BAC clones; the support of the technical staff of the Molecular Cytogenetic laboratories of the Institutes of Human Genetics in Kiel and Ulm; and Montserrat Puiggros from the Barcelona Supercomputing Center for support in WGS analysis. The authors also thank the contributors of individual cases: Iwona Wlodarska (Leuven, Belgium), Philippe Gaulard (Creteil, France), Wendy Erber (Crawley, Australia), Pilar Forcada (Terrassa, Spain), Grevelyn Sosa Rotundo (Madrid, Spain), Alejandra Carvajal (San Jose, Costa Rica), Camille Gonzalez (New York, NY), Nhora Silva Perez (Cali, Colombia), Lluís Rodríguez (Vic, Spain). The arrays were performed

at qGenomics ([www.qgenomics.com](http://www.qgenomics.com)), CeGen (PTI3/0001, ISCI-SCGFI/FEDER), and the IDIBAPS Genomics core facility. This work was developed at the Centro Esther Koplowitz (CEK), Barcelona, Spain.

This work was supported by research funding from Fondo de Investigaciones Sanitarias, Instituto de Salud Carlos III P114/00571 and P117/01061 (S. Beà); Fundació La Marató de TV3-Càncer/2013410 (S. Beà); Fundació Crèdit Andorrà, Ministerio de Economía y Competitividad, SAF2015-64885-R (E.C.); SAF2017-87811-R (X.S.P.) from Plan Nacional de I+D+I, Generalitat de Catalunya Suport Grups de Recerca 2017-SGR-709 (S. Beà); 2017-SGR-1142 (E.C.); and the European Regional Development Fund Una Manera de fer Europa, CERCA Programme/Generalitat de Catalunya. Personal staff (Miriam Prieto and Noelia García) are supported by Acció Instrumental d'Incorporació de Científics i Tecnòlegs PERIS 2016 (SLT002/16/00347 and SLT002/16/00336 from Generalitat de Catalunya).

E.C. is an academia researcher of the Institució Catalana de Recerca i Estudis Avançats of the Generalitat de Catalunya.

## Authorship

Contribution: E.C. and S. Beà designed the study; D.M.-G., R.V.-M., J.G.-A., D.T., S. Beltran, C.L.-O., X.S.P., and S. Beà analyzed and interpreted NGS data; A.N., M.P., R.W., G.R., S. Bens, B.E., D.C., R.S., and S. Beà performed and interpreted cytogenetic analysis; D.M.-G., A.N., M.P., I.S., and S. Beà performed and interpreted molecular studies; G.C. performed statistical analyses; I.R.-C., G.R., L.d.L., A.R., J.A.F., E.D.H., K.F., J.D., D.W., D.d.J., F.C., S.J.O., S.H.S., B.G.-F., L.V., E.M., G.O., L.Q.-M., E.S.J., and E.C. reviewed and collected IHC and pathological data; D.M.-G., A.N., E.C., and S. Beà wrote the manuscript; S. Beà directed and supervised the research; and all authors approved the final manuscript.

Conflict-of-interest disclosure: E.C. has received research funding from Gilead Sciences; has been a consultant for Takeda, Celgene, and Gilead; and is an author in a Lymphoma and Leukemia Molecular Profiling Project (LLMPP) patent "Method for selecting and treating lymphoma types" PCT/US14/64161. The remaining authors declare no competing financial interests.

ORCID profiles: D.M.-G., 0000-0002-0289-5915; G.C., 0000-0003-2588-7413; L.d.L., 0000-0003-3994-516X; J.D., 0000-0001-5023-0689; D.T., 0000-0002-6086-9037; S. Beltran, 0000-0002-2810-3445; L.Q.-M., 0000-0001-7156-5365; E.S.J., 0000-0003-4632-0301; I.S., 0000-0002-2427-9822; X.S.P., 0000-0001-9525-1483; E.C., 0000-0001-9850-9793; S. Beà, 0000-0001-7192-2385.

Correspondence: Sílvia Beà, Institut d'Investigacions Biomèdiques August Pi i Sunyer (IDIBAPS), Rosselló 149-153, 08036 Barcelona, Spain; e-mail: sbea@clinic.cat.

## Footnotes

Submitted 9 July 2018; accepted 1 December 2018. Prepublished online as *Blood* First Edition paper, 11 December 2018; DOI 10.1182/blood-2018-07-862151.

\*D.M.-G. and A.N. contributed equally to this study.

†X.S.P., E.C., and S. Beà contributed equally to this study.

The sequencing, expression, and copy-number array data reported in this article have been deposited in the European Genome-Phenome Archive (EGA; <http://www.ebi.ac.uk/ega/>), which is hosted at the European Bioinformatics Institute (EBI; accession number EGAS00001003060). Copy-number arrays of the cases included in Salaverria et al<sup>9</sup> have been previously deposited in the Gene Expression Omnibus database (accession number GSE42854).

The online version of this article contains a data supplement.

The publication costs of this article were defrayed in part by page charge payment. Therefore, and solely to indicate this fact, this article is hereby marked "advertisement" in accordance with 18 USC section 1734.

## REFERENCES

- Swerdlow SH, Campo E, Harris N, et al, eds. WHO Classification of Tumours of Haematopoietic and Lymphoid Tissues. Lyon, France: IARC; 2017.
- Jares P, Colomer D, Campo E. Molecular pathogenesis of mantle cell lymphoma. *J Clin Invest*. 2012;122(10):3416-3423.
- Royo C, Salaverria I, Hartmann EM, Rosenwald A, Campo E, Beà S. The complex landscape of genetic alterations in mantle cell lymphoma. *Semin Cancer Biol*. 2011;21(5):322-334.
- Fu K, Weisenburger DD, Greiner TC, et al; Lymphoma/Leukemia Molecular Profiling Project. Cyclin D1-negative mantle cell lymphoma: a clinicopathologic study based on gene expression profiling. *Blood*. 2005;106(13):4315-4321.
- Salaverria I, Royo C, Carvajal-Cuenca A, et al. CCND2 rearrangements are the most frequent genetic events in cyclin D1(-) mantle cell lymphoma. *Blood*. 2013;121(8):1394-1402.
- Gesk S, Klapper W, Martín-Subero JI, et al. A chromosomal translocation in cyclin D1-negative/cyclin D2-positive mantle cell lymphoma fuses the CCND2 gene to the IGH locus. *Blood*. 2006;108(3):1109-1110.
- Shiller SM, Zieske A, Holmes H III, Feldman AL, Law ME, Saad R. CD5-positive, cyclinD1-negative mantle cell lymphoma with a translocation involving the CCND2 gene and the IGL locus. *Cancer Genet*. 2011;204(3):162-164.
- Wlodarska I, Dierickx D, Vanhentenrijk V, et al. Translocations targeting CCND2, CCND3, and MYCN do occur in t(11;14)-negative mantle cell lymphomas. *Blood*. 2008;111(12):5683-5690.
- Herens C, Lambert F, Quintanilla-Martinez L, Bisig B, Deusings C, de Leval L. Cyclin D1-negative mantle cell lymphoma with cryptic t(12;14)(p13;q32) and cyclin D2 over-expression. *Blood*. 2008;111(3):1745-1746.
- Quintanilla-Martinez L, Slotta-Huspenina J, Koch I, et al. Differential diagnosis of cyclin D2+ mantle cell lymphoma based on fluorescence in situ hybridization and quantitative real-time-PCR. *Haematologica*. 2009;94(11):1595-1598.
- Mozos A, Royo C, Hartmann E, et al. SOX11 expression is highly specific for mantle cell lymphoma and identifies the cyclin D1-negative subtype. *Haematologica*. 2009;94(11):1555-1562.
- Hartmann EM, Campo E, Wright G, et al. Pathway discovery in mantle cell lymphoma by integrated analysis of high-resolution gene expression and copy number profiling. *Blood*. 2010;116(6):953-961.
- Ventura RA, Martín-Subero JI, Jones M, et al. FISH analysis for the detection of lymphoma-associated chromosomal abnormalities in routine paraffin-embedded tissue. *J Mol Diagn*. 2006;8(2):141-151.
- McGowan-Jordan J, Simons A, Schmid M, eds. ISCN 2016: An International System for Human Cytogenomic Nomenclature. Basel, Switzerland: S. Karger; 2016.
- Puente XS, Beà S, Valdés-Mas R, et al. Non-coding recurrent mutations in chronic lymphocytic leukaemia. *Nature*. 2015;526(7574):519-524.
- Beà S, Valdés-Mas R, Navarro A, et al. Landscape of somatic mutations and clonal evolution in mantle cell lymphoma. *Proc Natl Acad Sci USA*. 2013;110(45):18250-18255.
- Moncunill V, Gonzalez S, Beà S, et al. Comprehensive characterization of complex structural variations in cancer by directly comparing genome sequence reads. *Nat Biotechnol*. 2014;32(11):1106-1112.
- Layer RM, Chiang C, Quinlan AR, Hall IM. LUMPY: a probabilistic framework for structural variant discovery. *Genome Biol*. 2014;15(6):R84.
- Boeva V, Zinovyev A, Bleakley K, et al. Control-free calling of copy number alterations in deep-sequencing data using GC-content normalization. *Bioinformatics*. 2011;27(2):268-269.
- Puente XS, Pinyol M, Quesada V, et al. Whole-genome sequencing identifies recurrent mutations in chronic lymphocytic leukaemia. *Nature*. 2011;475(7354):101-105.
- Cibulskis K, Lawrence MS, Carter SL, et al. Sensitive detection of somatic point mutations in impure and heterogeneous cancer samples. *Nat Biotechnol*. 2013;31(3):213-219.
- Smyth GK. Linear models and empirical Bayes methods for assessing differential expression in microarray experiments. *Stat Appl Genet Mol Biol*. 2004;3:Article3.
- Beekman R, Chapaprieta V, Russiñol N, et al. The reference epigenome and regulatory chromatin landscape of chronic lymphocytic leukemia. *Nat Med*. 2018;24(6):868-880.
- Zhang J, Jima D, Moffitt AB, et al. The genomic landscape of mantle cell lymphoma is related to the epigenetically determined chromatin state of normal B cells. *Blood*. 2014;123(19):2988-2996.
- Royo C, Navarro A, Clot G, et al. Non-nodal type of mantle cell lymphoma is a specific biological and clinical subgroup of the disease. *Leukemia*. 2012;26(8):1895-1898.
- Clot G, Jares P, Gine E, et al. A gene signature that distinguishes conventional and leukemic nonnodal mantle cell lymphoma helps predict outcome. *Blood*. 2018;132(4):413-422.
- Sonoki T, Harder L, Horsman DE, et al. Cyclin D3 is a target gene of t(6;14)(p21.1;q32.3) of mature B-cell malignancies. *Blood*. 2001;98(9):2837-2844.
- Watanuki J, Hatakeyama K, Sonoki T, et al. Bone marrow large B cell lymphoma bearing cyclin D3 expression: clinical, morphologic, immunophenotypic, and genotypic analyses of seven patients. *Int J Hematol*. 2009;90(2):217-225.
- Wren D, Walker BA, Brüggemann M, et al; EuroClonality-NGS Consortium. Comprehensive translocation and clonality detection in lymphoproliferative disorders by next-generation sequencing. *Haematologica*. 2017;102(2):e57-e60.
- Solé F, Espinet B, Salido M, et al. Translocation t(6;14)(p12;q32): a novel cytogenetic abnormality in splenic lymphoma with villous lymphocytes. *Br J Haematol*. 2000;110(1):241-243.
- Tian E, Sawyer JR, Heuck CJ, et al. In multiple myeloma, 14q32 translocations are non-random chromosomal fusions driving high expression levels of the respective partner genes. *Genes Chromosomes Cancer*. 2014;53(7):549-557.
- Fonseca R, Bergsagel PL, Drach J, et al; International Myeloma Working Group. International Myeloma Working Group molecular classification of multiple myeloma: spotlight review. *Leukemia*. 2009;23(12):2210-2221.
- Ulvé R, Rault M, Bahin M, et al. Discovery of human-similar gene fusions in canine cancers. *Cancer Res*. 2017;77(21):5721-5727.
- Zimmerman MW, Liu Y, He S, et al. MYC drives a subset of high-risk pediatric neuroblastomas and is activated through mechanisms including enhancer hijacking and focal enhancer amplification. *Cancer Discov*. 2018;8(3):320-335.
- Valentijn LJ, Koster J, Zwijsen DA, et al. TERT rearrangements are frequent in neuroblastoma and identify aggressive tumors. *Nat Genet*. 2015;47(12):1411-1414.
- Northcott PA, Buchhalter I, Morrissy AS, et al. The whole-genome landscape of medulloblastoma subtypes. *Nature*. 2017;547(7663):311-317.
- Northcott PA, Lee C, Zichner T, et al. Enhancer hijacking activates GF11 family oncogenes in medulloblastoma. *Nature*. 2014;511(7510):428-434.
- Gröbner SN, Worst BC, Weischenfeldt J, et al; ICGC MMML-Seq Project. The landscape of genomic alterations across childhood cancers [published correction appears in *Nature*. 2018;559(7714):E10]. *Nature*. 2018;555(7696):321-327.
- Weischenfeldt J, Dubash T, Drinas AP, et al. Pan-cancer analysis of somatic copy-number alterations implicates IRS4 and IGF2 in enhancer hijacking. *Nat Genet*. 2017;49(1):65-74.
- Affer M, Chesi M, Chen WG, et al. Promiscuous MYC locus rearrangements hijack enhancers but mostly super-enhancers to dysregulate MYC expression in multiple myeloma. *Leukemia*. 2014;28(8):1725-1735.
- Chapuy B, Stewart C, Dunford AJ, et al. Molecular subtypes of diffuse large B cell lymphoma are associated with distinct pathogenic mechanisms and outcomes [published corrections appear in *Nat Med*. 2018;24(8):1292 and *Nat Med*. 2018;24(58):1290-1291]. *Nat Med*. 2018;24(5):679-690.
- Ryan RJ, Drier Y, Whitton H, et al. Detection of enhancer-associated rearrangements reveals mechanisms of oncogene dysregulation in B-cell lymphoma. *Cancer Discov*. 2015;5(10):1058-1071.
- Nagel I, Akasaka T, Klapper W, et al. Identification of the gene encoding cyclin E1 (CCNE1) as a novel IGH translocation partner in t(14;19)(q32;q12) in diffuse large B-cell

- lymphoma. *Haematologica*. 2009;94(7):1020-1023.
44. Spruck CH, Won KA, Reed SI. Deregulated cyclin E induces chromosome instability. *Nature*. 1999;401(6750):297-300.
  45. Hubalek MM, Widschwendter A, Erdel M, et al. Cyclin E dysregulation and chromosomal instability in endometrial cancer. *Oncogene*. 2004;23(23):4187-4192.
  46. Alsina M, Landolfi S, Aura C, et al. Cyclin E amplification/overexpression is associated with poor prognosis in gastric cancer. *Ann Oncol*. 2015;26(2):438-439.
  47. Scaltriti M, Eichhorn PJ, Cortés J, et al. Cyclin E amplification/overexpression is a mechanism of trastuzumab resistance in HER2+ breast cancer patients. *Proc Natl Acad Sci USA*. 2011;108(9):3761-3766.
  48. Frei E, Visco C, Xu-Monette ZY, et al. Addition of rituximab to chemotherapy overcomes the negative prognostic impact of cyclin E expression in diffuse large B-cell lymphoma. *J Clin Pathol*. 2013;66(11):956-961.
  49. Dictor M, Ek S, Sundberg M, et al. Strong lymphoid nuclear expression of SOX11 transcription factor defines lymphoblastic neoplasms, mantle cell lymphoma and Burkitt's lymphoma. *Haematologica*. 2009;94(11):1563-1568.
  50. Chen YH, Gao J, Fan G, Peterson LC. Nuclear expression of sox11 is highly associated with mantle cell lymphoma but is independent of t(11;14)(q13;q32) in non-mantle cell B-cell neoplasms. *Mod Pathol*. 2010;23(1):105-112.
  51. Hsiao SC, Cortada IR, Colomo L, et al. SOX11 is useful in differentiating cyclin D1-positive diffuse large B-cell lymphoma from mantle cell lymphoma. *Histopathology*. 2012;61(4):685-693.
  52. Soldini D, Valera A, Solé C, et al. Assessment of SOX11 expression in routine lymphoma tissue sections: characterization of new monoclonal antibodies for diagnosis of mantle cell lymphoma. *Am J Surg Pathol*. 2014;38(1):86-93.
  53. Xu S, Dong Y, Huo Z, et al. SOX11: a potentially useful marker in surgical pathology a systematic analysis of SOX11 expression in epithelial and nonepithelial tumors. *Histopathology*. 2019;74(3):391-405.
  54. Rosenquist R, Beà S, Du MQ, Nadel B, Pan-Hammarström Q. Genetic landscape and deregulated pathways in B-cell lymphoid malignancies. *J Intern Med*. 2017;282(5):371-394.
  55. Beà S, Amador V. Role of SOX11 and genetic events cooperating with cyclin D1 in mantle cell lymphoma. *Curr Oncol Rep*. 2017;19(6):43.